

Shape-constrained uncertainty quantification in unfolding steeply falling elementary particle spectra

Mikael Kuusela*

Institute of Mathematics

École Polytechnique Fédérale de Lausanne

`mikael.kuusela@epfl.ch`

Philip B. Stark

Department of Statistics

University of California, Berkeley

`stark@stat.berkeley.edu`

Abstract

The high energy physics unfolding problem is an important statistical inverse problem arising in data analysis at the Large Hadron Collider at CERN. The problem arises in making nonparametric inferences about a particle spectrum from measurements smeared by the finite resolution of the particle detectors. Existing unfolding methodology has major practical limitations stemming from ad hoc discretization and regularization of the problem. As a result, confidence intervals derived using the current methods can have significantly lower coverage than expected. In this work, we regularize the problem by imposing physically justified shape constraints. We quantify the uncertainty by constructing a nonparametric confidence set for the true spectrum consisting of all spectra that satisfy the shape constraints and that predict observations within an appropriately calibrated level of fit to the data. Projecting that set produces simultaneous confidence intervals for all functionals of the spectrum, including averages within bins. The confidence intervals have guaranteed frequentist finite-sample coverage in the important and challenging class of unfolding problems with steeply falling particle spectra. We demonstrate the efficacy of the method using simulations designed to mimic the unfolding of the inclusive jet transverse momentum spectrum at the Large Hadron Collider. The shape-constrained intervals provide usefully tight conservative confidence intervals, while the conventional methods suffer from major undercoverage.

Keywords: Poisson inverse problem, finite-sample coverage, high energy physics, Large Hadron Collider, Fenchel duality, semi-infinite programming

*Supported by the Swiss National Science Foundation grant no. 200021-153595.

1 Introduction

This paper studies shape-constrained statistical inference in the high energy physics *unfolding problem* (Prosper and Lyons, 2011; Cowan, 1998; Blobel, 2013; Kuusela and Panaretos, 2015). This is an important statistical inverse problem arising in data analysis at the Large Hadron Collider (LHC) at CERN, the European Organization for Nuclear Research. LHC measurements are affected by the finite resolution of the particle detectors. This causes the observations to be “smeared” or “blurred” versions of the true physical spectra. The unfolding problem is the inverse problem of making inferences about the true spectrum from the noisy, smeared observations.

The unfolding problem can be formalized using indirectly observed Poisson point processes (Kuusela and Panaretos, 2015). It is an ill-posed Poisson inverse problem (Antoniadis and Bigot, 2006; Reiss, 1993). Let M and N be Poisson point processes with intensity functions f_0 and g_0 and state spaces E and F , respectively. We assume that the state spaces are compact intervals of real numbers. Depending on the analysis, they could represent the energies, momenta, or production angles of particles. Let M represent the true, particle-level collision events and N the smeared, detector-level events. The intensity functions f_0 and g_0 are related by the Fredholm integral equation

$$g_0(t) = (Kf_0)(t) = \int_E k(t, s) f_0(s) ds, \quad t \in F. \quad (1)$$

The kernel $k(t, s)$ represents the response of the particle detector

$$k(t, s) = p(Y = t | X = s, X \text{ observed}) P(X \text{ observed} | X = s), \quad (2)$$

where X is a true, particle-level event and Y the corresponding smeared, detector-level event. In this paper, we take $k(t, s)$ to be known. The goal of unfolding is to make inferences about the true intensity f_0 from a single realization of the smeared process N .

Unfolding is used in dozens of LHC analyses annually. Existing unfolding methods, implemented in the ROOUNFOLD (Adye, 2011) software framework, have serious practical limitations. These algorithms first discretize the continuous problem in Equation (1) using histograms (Cowan, 1998, Chapter 11) and then regularize the ill-posed inverse problem either using expectation-maximization (EM) with early stopping (D’Agostini, 1995) or variants of Tikhonov regularization (Höcker and Kartvelishvili, 1996; Schmitt, 2012). Both approaches are ad hoc and produce biased estimates with uncertainties that can grossly underestimate the true uncertainty.

More specifically, let $\{E_i\}_{i=1}^p$ and $\{F_i\}_{i=1}^n$ be partitions of the true space E and the smeared space F , and let

$$\boldsymbol{\lambda} = \left[\int_{E_1} f_0(s) ds, \dots, \int_{E_p} f_0(s) ds \right]^T \text{ and } \boldsymbol{\mu} = \left[\int_{F_1} g_0(t) dt, \dots, \int_{F_n} g_0(t) dt \right]^T \quad (3)$$

be the expected number of true events and of smeared events in each bin, respectively. The two are related by $\boldsymbol{\mu} = \mathbf{K}\boldsymbol{\lambda}$, where the elements of the response matrix \mathbf{K} are

$$K_{i,j} = \frac{\int_{F_i} \int_{E_j} k(t,s) f_0(s) \, ds \, dt}{\int_{E_j} f_0(s) \, ds}, \quad i = 1, \dots, n, \quad j = 1, \dots, p. \quad (4)$$

The response matrix depends on the shape of the true intensity f_0 within each true bin. In practice, f_0 is unknown; after all, the problem is to infer it. The matrix \mathbf{K} is hence constructed numerically by replacing f_0 with a simulated prediction obtained using a Monte Carlo (MC) event generator. In this discretization, unfolding becomes estimating $\boldsymbol{\lambda}$ in the Poisson regression problem $\mathbf{y} \sim \text{Poisson}(\mathbf{K}\boldsymbol{\lambda})$, where $\mathbf{y} = [N(F_1), \dots, N(F_n)]^T$ is the vector of bin counts corresponding to the histogram of smeared observations.

The Tikhonov-regularized unfolding techniques then make a Gaussian approximation to the Poisson likelihood and estimate $\boldsymbol{\lambda}$ by solving the optimization problem

$$\min_{\boldsymbol{\lambda} \in \mathbb{R}^p} (\mathbf{y} - \mathbf{K}\boldsymbol{\lambda})^T \hat{\mathbf{C}}^{-1} (\mathbf{y} - \mathbf{K}\boldsymbol{\lambda}) + \delta P(\boldsymbol{\lambda}), \quad (5)$$

where $\hat{\mathbf{C}} = \text{diag}(\mathbf{y})$ is an estimate of the covariance of \mathbf{y} , $\delta > 0$ is a regularization parameter, and $P(\boldsymbol{\lambda})$ is a penalty term to regularize the otherwise ill-posed problem. Two Tikhonov-regularized unfolding techniques are common in LHC data analysis: The TUNFOLD variant (Schmitt, 2012) uses the penalty term $P(\boldsymbol{\lambda}) = \|\mathbf{L}(\boldsymbol{\lambda} - \boldsymbol{\lambda}^{\text{MC}})\|_2^2$, where \mathbf{L} is a discretized second derivative operator and $\boldsymbol{\lambda}^{\text{MC}}$ is a Monte Carlo prediction of $\boldsymbol{\lambda}$. The SVD variant (with SVD standing for the singular value decomposition, Höcker and Kartvelishvili (1996)) replaces the difference $\boldsymbol{\lambda} - \boldsymbol{\lambda}^{\text{MC}}$ with the binwise ratios of $\boldsymbol{\lambda}$ and $\boldsymbol{\lambda}^{\text{MC}}$. EM with early stopping (D’Agostini, 1995) starts the iteration from $\boldsymbol{\lambda}^{\text{MC}}$ and then stops before convergence to regularize the solution (iteration to convergence produces undesired oscillations). All these methods regularize the problem by biasing the solution towards a Monte Carlo prediction of $\boldsymbol{\lambda}$. The uncertainty of the resulting point estimate $\hat{\boldsymbol{\lambda}}$ is then quantified by estimating its binwise standard errors using error propagation, ignoring the discretization and regularization bias.

The biggest problem with the current unfolding methods is that their uncertainty estimates are unrealistically small. In high energy physics applications, it is crucial to be able to construct confidence intervals with good frequentist coverage properties. But it is well understood that constructing confidence intervals using only the variability of a point estimate generally leads to undercoverage, since this ignores all the biases. These issues have been studied extensively in the spline smoothing literature (see, e.g., Rupert et al. (2003, Chapter 6)). Kuusela and Panaretos (2015) show that standard uncertainty quantification techniques can lead to dramatic undercoverage in the unfolding problem. Moreover, using Monte Carlo prediction

first to discretize and then to regularize the problem introduces an unnecessary model-dependence with additional uncertainty that is extremely difficult to quantify rigorously.

Spectra that fall steeply over many orders of magnitude are especially difficult to estimate well. For such spectra, the response matrix \mathbf{K} depends strongly on the assumed Monte Carlo model, since the spectrum varies substantially within each true bin. Current techniques regularize estimates of such spectra by requiring the unfolded solution to be close to a steeply falling Monte Carlo prediction. Trying to reduce the Monte Carlo dependence by using a global second-derivative penalty that does not depend on λ^{MC} does not work well because the true solution has a highly heterogeneous second derivative, large on the left and a small on the right.

Unfortunately, energy and transverse momentum spectra of particle interactions are usually steeply falling. Recent LHC analyses that involve unfolding such spectra include the measurement of the differential cross section of jets (CMS Collaboration, 2013b), top quark pairs (CMS Collaboration, 2013a), the W boson (ATLAS Collaboration, 2012) and the Higgs boson (CMS Collaboration, 2015). Expected key outcomes of LHC Run II, currently underway, include more precise measurements of these and related steeply falling differential cross sections. A better method for unfolding such spectra is needed.

This paper develops a new method for forming rigorous confidence intervals in the unfolding problem using an approach that is particularly well-suited to steeply falling spectra. Instead of regularizing using a roughness penalty, we use shape constraints in the form of positivity, monotonicity, and convexity. Such constraints are an intuitive and physically justified way to regularize a wide range of unfolding analyses, including those mentioned above, without the need to bias the solution towards a Monte Carlo prediction nor to choose a regularization parameter δ . The use of shape constraints to estimate a steeply falling spectrum is demonstrated in Figure 1(a).

Shape constraints are easy to incorporate into uncertainty quantification using the *strict bounds* approach (Stark, 1992), which constructs simultaneous confidence intervals by solving optimization problems over the set of all functions that satisfy the shape constraints and agree adequately with the data (the misfit criterion and misfit level are chosen to give the desired coverage probability). For the unfolding problem, the intervals are computed using a semi-discrete forward mapping, allowing the spectrum to vary arbitrarily with the true bins, subject only to the shape constraints. This approach enables us to form confidence intervals for λ that provide *guaranteed, finite-sample, joint frequentist coverage* without the model-dependence and discretization and regularization biases of existing methods. Figure 1(b) shows the resulting intervals for the inclusive jet transverse momentum spectrum studied in Section 4. Deriving such intervals and presenting methods to compute them are the main contributions of this paper. To do so, we

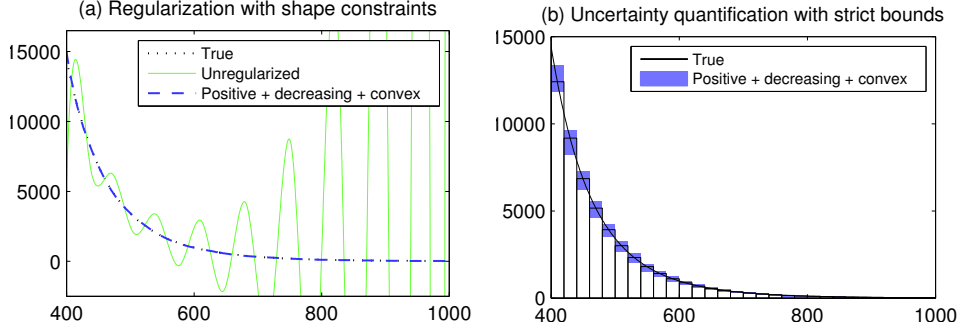


Figure 1: Unfolding a steeply falling elementary particle spectrum (see Section 4 for a description of the data). The solid curve in Figure (a) demonstrates the ill-posedness of the problem by showing a typical unregularized solution (here, a cubic spline that maximizes the likelihood). Shape constraints provide a natural way to rule out such unphysical solutions. If the solution is constrained to be positive, decreasing and convex (dashed line), it becomes hard to distinguish it from the true spectrum (dotted line). We form confidence intervals for the unfolded spectrum by considering all functions that satisfy the shape constraints and fit the observations within a tolerance calibrated to give the specified confidence level. The resulting 95 % shape-constrained simultaneous confidence intervals are shown in Figure (b). By construction, the finite-sample joint coverage probability of these intervals is guaranteed to be at least 95 %.

extend the strict bounds methodology of Stark (1992) and Hengartner and Stark (1995) by considering Poisson noise and a new way of imposing the monotonicity and convexity constraints. We also introduce a novel way of conservatively discretizing the resulting semi-infinite optimization problems.

Section 2 outlines the proposed inference method. Section 3 explains how to construct the shape-constrained strict bounds. Section 4 illustrates the bounds in a simulation study and demonstrates that the existing methods can fail to achieve their nominal coverage, even in a very common unfolding scenario. Section 5 concludes. Appendices give derivations and implementation details.

2 Outline of the methodology

Let V denote the space of (sufficiently regular) functions on the compact interval $E \subset \mathbb{R}$. The discrete random measure M on state space E is a *Poisson point process* (Reiss, 1993) with a nonnegative intensity function $f \in V$ if and only if

1. $M(B) \sim \text{Poisson}(\lambda(B))$ with $\lambda(B) = \int_B f(s) ds$ for every Borel set $B \subset E$;

2. $M(B_1), \dots, M(B_n)$ are independent for pairwise disjoint Borel sets $B_i \subset E$, $i = 1, \dots, n$.

In the unfolding problem, the true, particle-level observations are a realization of such a Poisson point process M on state space E with intensity function f_0 . Let W denote the space of (sufficiently regular) functions on the compact interval $F \subset \mathbb{R}$. The smeared, detector-level observations are a realization of the Poisson point process N on state space F with a non-negative intensity function $g_0 \in W$. The two intensity functions are related by $g_0 = K f_0$, where the forward operator $K : V \rightarrow W$ is defined by Equation (1).

High energy physics data are typically binned, both for convenience and computational tractability. Indeed, for steeply falling spectra, the leftmost bins may contain billions of observations: treating them individually would not be computationally feasible. We assume that the smeared observations are counts in bins $\mathbf{y} \equiv [N(F_1), \dots, N(F_n)]^T$, where $\{F_j\}_{j=1}^n$ is a binning of the smeared space F :

$$F_j \equiv \begin{cases} [F_{j,\min}, F_{j,\max}), & j = 1, \dots, n-1, \\ [F_{j,\min}, F_{j,\max}], & j = n, \end{cases} \quad (6)$$

with $F_{j,\max} = F_{j+1,\min}$, $j = 1, \dots, n-1$. The mean vector of these counts is $\boldsymbol{\mu} \equiv \left[\int_{F_1} g_0(t) dt, \dots, \int_{F_n} g_0(t) dt \right]^T$, which has components

$$\mu_j = \int_{F_j} \int_E k(t, s) f_0(s) ds dt = \int_E k_j(s) f_0(s) ds \equiv K_j f_0, \quad j = 1, \dots, n, \quad (7)$$

where $k_j(s) \equiv \int_{F_j} k(t, s) dt$. We assume here and below that f_0 and k are sufficiently regular that we can interchange the order of integration. Let \mathcal{K} denote the semi-discrete linear operator that maps a particle-level intensity function f to the detector-level mean vector $\boldsymbol{\mu}$:

$$\mathcal{K} : V \rightarrow \mathbb{R}^n, \quad f \mapsto [K_1 f, \dots, K_n f]^T. \quad (8)$$

Our statistical model hence becomes

$$\mathbf{y} \sim \text{Poisson}(\boldsymbol{\mu}), \quad \text{with } \boldsymbol{\mu} = \mathcal{K} f_0, \quad (9)$$

with the components of \mathbf{y} independent.

We seek confidence intervals for the binned means of the true process M :

$$\boldsymbol{\lambda} \equiv \left[\int_{E_1} f_0(s) ds, \dots, \int_{E_p} f_0(s) ds \right]^T = [H_1 f_0, \dots, H_p f_0]^T, \quad (10)$$

where $\{E_k\}_{k=1}^p$ is a partition of E into intervals and, for each $k = 1, \dots, p$, $H_k f \equiv \int_{E_k} f(s) ds$. As before, the partition is of the form

$$E_k \equiv \begin{cases} [E_{k,\min}, E_{k,\max}), & k = 1, \dots, p-1, \\ [E_{k,\min}, E_{k,\max}], & k = p, \end{cases} \quad (11)$$

with $E_{k,\max} = E_{k+1,\min}$, $k = 1, \dots, p-1$.

Instead of further discretizing the forward mapping, we construct confidence intervals using *strict bounds*, following Stark (1992):

1. For fixed $\alpha \in (0, 1)$, let $\Xi \subset \mathbb{R}^n$ be a $1 - \alpha$ joint confidence set for $\boldsymbol{\mu}$ in the smeared space, so that $P_{f_0}\{\Xi \ni \boldsymbol{\mu}\} \geq 1 - \alpha$.
2. The preimage $D \equiv \mathcal{K}^{-1}(\Xi)$ of Ξ under the mapping \mathcal{K} is a $1 - \alpha$ confidence set for the (infinite-dimensional, not discretized) particle-level intensity function f_0 : $P_{f_0}\{D \ni f_0\} \geq 1 - \alpha$.
3. Let $C \subset V$ denote the set of functions that satisfy the shape constraints. If $f_0 \in C$, then $C \cap D$ is also a $1 - \alpha$ confidence set for f_0 : $P_{f_0}\{C \cap D \ni f_0\} \geq 1 - \alpha$.
4. Whenever $f_0 \in C \cap D$ (which occurs with probability at least $1 - \alpha$), any condition that holds for every $f \in C \cap D$ holds for f_0 . In particular, $H_k f_0 \geq \inf_{f \in C \cap D} H_k f \equiv \underline{\lambda}_k$ and $H_k f_0 \leq \sup_{f \in C \cap D} H_k f \equiv \bar{\lambda}_k$, for every k . Each interval $[\underline{\lambda}_k, \bar{\lambda}_k]$ is a $1 - \alpha$ confidence interval for λ_k . Moreover, the set $[\underline{\lambda}_1, \bar{\lambda}_1] \times \dots \times [\underline{\lambda}_p, \bar{\lambda}_p] \subset \mathbb{R}^p$ is a $1 - \alpha$ joint confidence set for $\boldsymbol{\lambda}$: Whenever $C \cap D$ covers f_0 , the p intervals $\{[\underline{\lambda}_j, \bar{\lambda}_j]\}_{j=1}^p$ all cover the corresponding components of $\boldsymbol{\lambda}$.

This construction is illustrated schematically in Figure 2.

The joint coverage probability of $[\underline{\lambda}_1, \bar{\lambda}_1] \times \dots \times [\underline{\lambda}_p, \bar{\lambda}_p]$ can be greater than that of $C \cap D$: there are elements of that set that do not correspond to any $C \cap D$. Thus, the intervals are guaranteed to have joint confidence level at least $1 - \alpha$, but the actual coverage probability might be much larger.

Constructing confidence intervals involves solving the optimization problems $\inf_{f \in C \cap D} H_k f$ and $\sup_{f \in C \cap D} H_k f$. Since

$$\sup_{f \in C \cap D} H_k f = - \inf_{f \in C \cap D} -H_k f, \quad (12)$$

we focus on the minimization problem, without loss of generality. We cannot directly solve the infinite-dimensional optimization problem $\inf_{f \in C \cap D} H_k f$. Instead, we follow the approach of Stark (1992) and use Fenchel duality to bound $\inf_{f \in C \cap D} H_k f$ from below by a semi-infinite program with an n -dimensional unknown and an infinite set of constraints. We discretize the constraints in such a way that every feasible point for the discretized finite-dimensional dual program is a lower bound for the original program $\inf_{f \in C \cap D} H_k f$, ensuring that the joint confidence level of the resulting intervals is at least $1 - \alpha$.

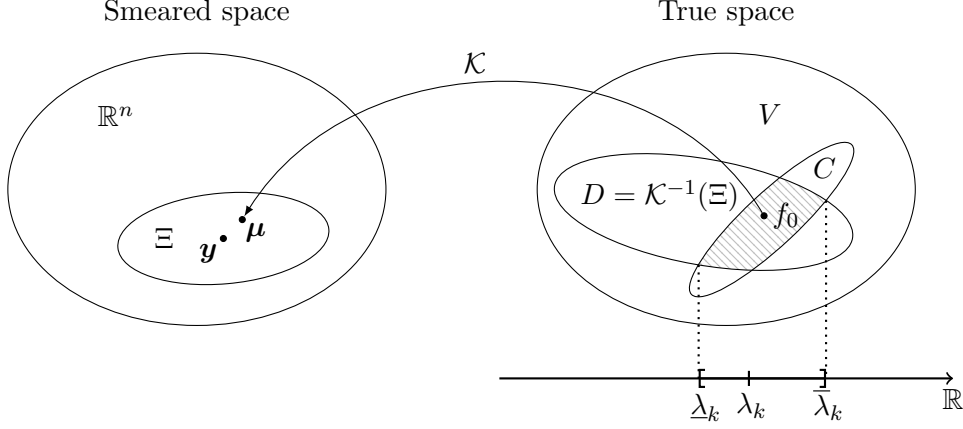


Figure 2: Schematic of strict bounds confidence intervals. The set Ξ in the smeared space is a confidence set for μ based on y . Its preimage $D = \mathcal{K}^{-1}(\Xi)$ is a confidence set for f_0 . If f_0 satisfies the shape constraints C , then $C \cap D$ is also a confidence set for f_0 . The confidence intervals are the extremal values of the functionals of interest over $C \cap D$.

3 Shape-constrained unfolding

This section explains in detail how to compute the shape-constrained strict bounds in the unfolding problem. Section 3.1 develops the confidence set Ξ for the smeared mean μ . Section 3.2 applies Fenchel duality to turn the infinite-dimensional program $\inf_{f \in C \cap D} H_k f$ into a semi-infinite program, whose explicit form for various shape constraints is derived in Section 3.3. Finally, Section 3.4 explains how to discretize the semi-infinite program in such a way that the confidence level is preserved.

3.1 Confidence set in the smeared space

Constructing the confidence set Ξ for the mean μ in the model $y \sim \text{Poisson}(\mu)$ is straightforward because the counts in disjoint bins are independent. For each $j = 1, \dots, n$ and for $\alpha' \in (0, 1)$, let $[\underline{\mu}_{j,\alpha'}, \bar{\mu}_{j,\alpha'}]$ be a $1 - \alpha'$ confidence interval for μ_j constructed using y_j only. Then $\mathbb{P}_{f_0}(\underline{\mu}_{1,\alpha'} \leq \mu_1 \leq \bar{\mu}_{1,\alpha'}, \dots, \underline{\mu}_{n,\alpha'} \leq \mu_n \leq \bar{\mu}_{n,\alpha'}) = \prod_{j=1}^n \mathbb{P}_{f_0}(\underline{\mu}_{j,\alpha'} \leq \mu_j \leq \bar{\mu}_{j,\alpha'}) \geq (1 - \alpha')^n$. Hence, $\Xi = [\underline{\mu}_{1,\alpha'}, \bar{\mu}_{1,\alpha'}] \times \dots \times [\underline{\mu}_{n,\alpha'}, \bar{\mu}_{n,\alpha'}]$ becomes a $1 - \alpha$ confidence set for μ with the choice $\alpha' = 1 - (1 - \alpha)^{1/n}$ for $\alpha \in (0, 1)$.

The binwise confidence intervals $[\underline{\mu}_{j,\alpha'}, \bar{\mu}_{j,\alpha'}]$ can be formed using the Garwood construction (Garwood, 1936). That is, for each bin with a nonzero event count, the bounds are given by

$$\underline{\mu}_{j,\alpha'} = \frac{1}{2} F_{\chi^2}^{-1} \left(\frac{\alpha'}{2}; 2y_j \right) \quad \text{and} \quad \bar{\mu}_{j,\alpha'} = \frac{1}{2} F_{\chi^2}^{-1} \left(1 - \frac{\alpha'}{2}; 2(y_j + 1) \right), \quad (13)$$

where $F_{\chi^2}^{-1}(\cdot; k)$ denotes the inverse cumulative distribution function of the χ^2 distribution with k degrees of freedom. If $y_j = 0$, the upper bound $\bar{\mu}_{j,\alpha'}$ is still given by Equation (13), while the lower bound $\underline{\mu}_{j,\alpha'}$ is zero. These intervals are guaranteed to have confidence level $1 - \alpha'$, although the actual coverage probability is strictly greater than that for any finite μ_j , an unavoidable consequence of the discreteness of the Poisson distribution.

For what follows, it is useful to write the hyperrectangle Ξ using its center point, that is, $\Xi = \{\tilde{\mathbf{y}} + \boldsymbol{\xi} \in \mathbb{R}^n : \|\text{diag}(\mathbf{l})^{-1}\boldsymbol{\xi}\|_\infty \leq 1\}$, where, for each $j = 1, \dots, n$, $\tilde{y}_j = (\underline{\mu}_{j,\alpha'} + \bar{\mu}_{j,\alpha'})/2$ and $l_j = (\bar{\mu}_{j,\alpha'} - \underline{\mu}_{j,\alpha'})/2$.

3.2 Strict bounds via duality

To be able to compute the lower bound $p = \inf_{f \in C \cap D} H_k f$, we follow the approach of Stark (1992) and apply Fenchel duality. The Fenchel dual (Luenberger, 1969, Section 7.12) of the problem is given by

$$d = \sup_{f^* \in C^* \cap D^*} \left\{ \inf_{f \in D} f^*[f] + \inf_{f \in C} (H_k - f^*)[f] \right\}, \quad (14)$$

where $C^* = \{f^* \in V^* : \inf_{f \in C} (H_k - f^*)[f] > -\infty\}$ and $D^* = \{f^* \in V^* : \inf_{f \in D} f^*[f] > -\infty\}$ and V^* is the algebraic dual space of V , that is, the set of all linear functionals on V . The two problems satisfy weak duality, $p \geq d$, and, when strict inequality holds, solving the dual problem gives a conservative lower bound. Under regularity conditions (see Luenberger (1969, Section 7.12) and Stark (1992, Section 10.1)), one can establish strong duality, $p = d$, in which case the dual gives a tight bound.

The beauty of the Fenchel dual is that it can be written using a finite-dimensional unknown. Namely, the set D^* consists of functionals that are linear combinations of the forward functionals K_j , $D^* = \{f^* \in V^* : f^* = \boldsymbol{\nu} \cdot \mathcal{K}, \boldsymbol{\nu} \in \mathbb{R}^n\}$ (Stark, 1992; Backus, 1970), where $\boldsymbol{\nu} \cdot \mathcal{K} \equiv \sum_{j=1}^n \nu_j K_j$. The dual problem becomes

$$d = \sup_{\boldsymbol{\nu} \in \mathbb{R}^n : \boldsymbol{\nu} \cdot \mathcal{K} \in C^*} \left\{ \inf_{f \in D} (\boldsymbol{\nu} \cdot \mathcal{K})[f] + \inf_{f \in C} (H_k - \boldsymbol{\nu} \cdot \mathcal{K})[f] \right\}. \quad (15)$$

Here the first term can be expressed in a closed form: when $f \in D$,

$$\begin{aligned} (\boldsymbol{\nu} \cdot \mathcal{K})[f] &= \boldsymbol{\nu}^T (\tilde{\mathbf{y}} + \boldsymbol{\xi}) \geq \boldsymbol{\nu}^T \tilde{\mathbf{y}} - |\boldsymbol{\nu}^T \boldsymbol{\xi}| \\ &= \boldsymbol{\nu}^T \tilde{\mathbf{y}} - |(\text{diag}(\mathbf{l})\boldsymbol{\nu})^T (\text{diag}(\mathbf{l})^{-1}\boldsymbol{\xi})| \\ &\geq \boldsymbol{\nu}^T \tilde{\mathbf{y}} - \|\text{diag}(\mathbf{l})\boldsymbol{\nu}\|_1 \|\text{diag}(\mathbf{l})^{-1}\boldsymbol{\xi}\|_\infty \\ &\geq \boldsymbol{\nu}^T \tilde{\mathbf{y}} - \|\boldsymbol{\nu}\|_1^l, \end{aligned} \quad (16)$$

where we have used the notation $\|\boldsymbol{\nu}\|_1^l \equiv \|\text{diag}(\mathbf{l})\boldsymbol{\nu}\|_1$ for the weighted 1-norm. Hence,

$$\inf_{f \in D} (\boldsymbol{\nu} \cdot \mathcal{K})[f] \geq \boldsymbol{\nu}^T \tilde{\mathbf{y}} - \|\boldsymbol{\nu}\|_1^l. \quad (17)$$

When the forward functionals K_j are linearly independent, an argument similar to that of Stark (1992, Section 5) shows that the lower bound in Equation (17) is in fact sharp.

To summarize, we have established the inequality

$$\inf_{f \in C \cap D} H_k f \geq \sup_{\boldsymbol{\nu} \in \mathbb{R}^n : \boldsymbol{\nu} \cdot \mathcal{K} \in C^*} \left\{ \boldsymbol{\nu}^T \tilde{\mathbf{y}} - \|\boldsymbol{\nu}\|_1^l + \inf_{f \in C} (H_k - \boldsymbol{\nu} \cdot \mathcal{K})[f] \right\}, \quad (18)$$

which holds as an equality under regularity conditions. If the regularity conditions are not satisfied, the solution of the dual problem still gives a valid but possibly conservative bound.

We next turn our attention to the last term in Equation (18). For all shape constraints we consider, C is a convex cone. In other words, the set C is convex and if $f \in C$, then $\gamma f \in C$ for all $\gamma \geq 0$. It then follows from Stark (1992, Section 6.2) that

$$\begin{aligned} C^* &= \{f^* \in V^* : \inf_{f \in C} (H_k - f^*)[f] = 0\} \\ &= \{f^* \in V^* : (H_k - f^*)[f] \geq 0, \forall f \in C\}, \end{aligned} \quad (19)$$

in which case the dual problem simplifies to

$$\sup_{\boldsymbol{\nu} \in \mathbb{R}^n} \left\{ \boldsymbol{\nu}^T \tilde{\mathbf{y}} - \|\boldsymbol{\nu}\|_1^l \right\} \quad \text{subject to} \quad (H_k - \boldsymbol{\nu} \cdot \mathcal{K})[f] \geq 0, \forall f \in C. \quad (20)$$

Finding the lower bound hence becomes a semi-infinite program with an n -dimensional free variable and an infinite set of inequality constraints.

3.3 Constraints of the dual program

We consider the following shape constraints C for the true intensity f :

- (P) f is positive;
- (D) f is positive and decreasing;
- (C) f is positive, decreasing and convex.

The positivity constraint is true for any intensity function f , while the monotonicity and convexity constraints are motivated by shapes typically observed in steeply falling particle spectra. In this section, we give the explicit form of the constraint $(H_k - \boldsymbol{\nu} \cdot \mathcal{K})[f] \geq 0, \forall f \in C$, for each of these

shapes. Let us start by rewriting the left-hand side:

$$(H_k - \boldsymbol{\nu} \cdot \mathcal{K})[f] = H_k f - \sum_{j=1}^n \nu_j K_j f \quad (21)$$

$$= \int_{E_k} f(s) \, ds - \sum_{j=1}^n \nu_j \int_E k_j(s) f(s) \, ds \quad (22)$$

$$= \int_E \underbrace{\left(\mathbf{1}_{E_k}(s) - \sum_{j=1}^n \nu_j k_j(s) \right)}_{:= h_k(s)} f(s) \, ds = \int_E h_k(s) f(s) \, ds. \quad (23)$$

Hence the dual constraint becomes $\int_E h_k(s) f(s) \, ds \geq 0$ for all $f \in C$, where $h_k(s) = \mathbf{1}_{E_k}(s) - \sum_{j=1}^n \nu_j k_j(s)$ and $\mathbf{1}_{E_k}$ denotes the indicator function of E_k .

For simplicity, we assume that the space V consists of twice continuously differentiable functions on E and note that this assumption can be relaxed, at least for the constraints (P) and (D). We furthermore assume that the k_j are continuous which implies that h_k is right-continuous. Denote the endpoints of the interval E by E_{\min} and E_{\max} . For each shape constraint, the dual constraint can be equivalently written as a constraint on h_k :

$$(P) \quad h_k(s) \geq 0, \quad \forall s \in E;$$

$$(D) \quad \int_{E_{\min}}^s h_k(s') \, ds' \geq 0, \quad \forall s \in E;$$

$$(C) \quad \int_{E_{\min}}^s \int_{E_{\min}}^{s'} h_k(s'') \, ds'' \, ds' \geq 0, \quad \forall s \in E \text{ and } \int_E h_k(s) \, ds \geq 0.$$

The result for the positivity constraint (P) follows directly, while the results (D) and (C) follow from integration by parts and are derived in Appendix A. On substituting the definition of h_k from Equation (23), we find the following constraints for $\boldsymbol{\nu}$ in the optimization problem $\sup_{\boldsymbol{\nu} \in \mathbb{R}^n} \{ \boldsymbol{\nu}^T \tilde{\mathbf{y}} - \|\boldsymbol{\nu}\|_1^t \}$:

$$(P) \quad \sum_{j=1}^n \nu_j k_j(s) \leq L_k^P(s), \quad \forall s \in E;$$

$$(D) \quad \sum_{j=1}^n \nu_j k_j^*(s) \leq L_k^D(s), \quad \forall s \in E;$$

$$(C) \quad \sum_{j=1}^n \nu_j k_j^{**}(s) \leq L_k^C(s), \quad \forall s \in E \text{ and } \sum_{j=1}^n \nu_j k_j^*(E_{\max}) \leq E_{k,\max} - E_{k,\min},$$

where $k_j^*(s) = \int_{E_{\min}}^s k_j(s') ds'$, $k_j^{**}(s) = \int_{E_{\min}}^s \int_{E_{\min}}^{s'} k_j(s'') ds'' ds'$ and the bounding functions on the right-hand side are

$$L_k^P(s) = \mathbf{1}_{E_k}(s), \quad (24)$$

$$L_k^D(s) = \begin{cases} 0, & s \leq E_{k,\min}, \\ s - E_{k,\min}, & E_{k,\min} < s \leq E_{k,\max}, \\ E_{k,\max} - E_{k,\min}, & s > E_{k,\max}, \end{cases} \quad (25)$$

$$L_k^C(s) = \begin{cases} 0, & s \leq E_{k,\min}, \\ \frac{1}{2}(s - E_{k,\min})^2, & E_{k,\min} < s \leq E_{k,\max}, \\ \frac{1}{2}(E_{k,\max} - E_{k,\min})^2 + (E_{k,\max} - E_{k,\min})(s - E_{k,\max}), & s > E_{k,\max}. \end{cases} \quad (26)$$

For positivity, the constraint is piecewise constant; for monotonicity, it consists of two constant parts connected by a linear part; and for convexity, it has a constant and a linear part connected by a quadratic part.

We have hence found explicit expressions for the constraints of the semi-infinite dual program corresponding to the lower bound $\underline{\lambda}_k = \inf_{f \in C \cap D} H_k f$. Similar reasoning shows that the upper bound $\bar{\lambda}_k = \sup_{f \in C \cap D} H_k f = -\inf_{f \in C \cap D} -H_k f$ is bounded from above by $\inf_{\nu \in \mathbb{R}^n} -\{\nu^T \tilde{g} - \|\nu\|_1^l\}$ subject to the constraints:

$$(P) \quad \sum_{j=1}^n \nu_j k_j(s) \leq -L_k^P(s), \quad \forall s \in E;$$

$$(D) \quad \sum_{j=1}^n \nu_j k_j^*(s) \leq -L_k^D(s), \quad \forall s \in E;$$

$$(C) \quad \sum_{j=1}^n \nu_j k_j^{**}(s) \leq -L_k^C(s), \quad \forall s \in E \text{ and } \sum_{j=1}^n \nu_j k_j^*(E_{\max}) \leq E_{k,\min} - E_{k,\max}.$$

3.4 Discretization of the dual constraints

To be able to compute the values of the dual bounds, we need to discretize the infinite set of constraints. To do so, introduce a grid $\{s_i\}_{i=1}^{m+1}$ on E consisting of $m+1$ grid points with $m \gg p$. We assume that $s_1 = E_{\min}$, $s_{m+1} = E_{\max}$ and that there is a grid point at each boundary between the true bins $\{E_k\}_{k=1}^p$.

Imagine discretizing the constraints just by imposing them at the grid points $\{s_i\}_{i=1}^{m+1}$. For example, the discretized version of the constraint (P) for the lower bound would be

$$\sum_{j=1}^n \nu_j k_j(s_i) \leq L_k^P(s_i), \quad i = 1, \dots, m+1. \quad (27)$$

This is not conservative: the feasible set of the discretized constraint of Equation (27) is larger than that of the original constraint, so the resulting confidence interval could be too short.

To guarantee the confidence level, we need to discretize the constraints in such a way that the discretized feasible set is a subset of the original feasible set. We use the grid $\{s_i\}_{i=1}^{m+1}$ to find a convenient upper bound for the left-hand side of the constraints and then make sure that this upper bound lies below the constraint functions $\pm L_k^P$, $\pm L_k^D$ or $\pm L_k^C$.

Consider the constraint (P) for the lower bound. For each $j = 1, \dots, n$, let us write $\nu_j = \nu_j^+ - \nu_j^-$ with $\nu_j^+, \nu_j^- \geq 0$. Now, for every $s \in [s_i, s_{i+1})$,

$$\begin{aligned} \sum_{j=1}^n \nu_j k_j(s) &= \sum_{j=1}^n \nu_j^+ k_j(s) - \sum_{j=1}^n \nu_j^- k_j(s) \\ &\leq \sum_{j=1}^n \nu_j^+ \underbrace{\sup_{\xi \in [s_i, s_{i+1})} k_j(\xi)}_{:= \bar{\rho}_{i,j}} - \sum_{j=1}^n \nu_j^- \underbrace{\inf_{\xi \in [s_i, s_{i+1})} k_j(\xi)}_{:= \underline{\rho}_{i,j}} \\ &= \sum_{j=1}^n \nu_j^+ \bar{\rho}_{i,j} - \sum_{j=1}^n \nu_j^- \underline{\rho}_{i,j}. \end{aligned} \quad (28)$$

This bounds the left-hand side by a constant with respect to s on the interval $[s_i, s_{i+1})$. Arrange the scalars $\bar{\rho}_{i,j}$ and $\underline{\rho}_{i,j}$ into the matrix

$$\mathbf{A} = \begin{bmatrix} \bar{\rho}_{1,1} & \cdots & \bar{\rho}_{1,n} & -\underline{\rho}_{1,1} & \cdots & -\underline{\rho}_{1,n} \\ \vdots & \ddots & \vdots & \vdots & \ddots & \vdots \\ \bar{\rho}_{m,1} & \cdots & \bar{\rho}_{m,n} & -\underline{\rho}_{m,1} & \cdots & -\underline{\rho}_{m,n} \end{bmatrix}. \quad (29)$$

Write

$$\tilde{\boldsymbol{\nu}} = \begin{bmatrix} \boldsymbol{\nu}^+ \\ \boldsymbol{\nu}^- \end{bmatrix} \quad \text{with} \quad \boldsymbol{\nu}^+ = \begin{bmatrix} \nu_1^+ \\ \vdots \\ \nu_n^+ \end{bmatrix} \quad \text{and} \quad \boldsymbol{\nu}^- = \begin{bmatrix} \nu_1^- \\ \vdots \\ \nu_n^- \end{bmatrix} \quad (30)$$

and let $\mathbf{b}_k^P \in \mathbb{R}^m$ denote the vector with components $b_{k,i}^P = L_k^P(s_i) = \mathbf{1}_{E_k}(s_i)$, $i = 1, \dots, m$. Then the constraint $\mathbf{A}\tilde{\boldsymbol{\nu}} \leq \mathbf{b}_k^P$ is a conservative discretization of the original dual constraint $\sum_{j=1}^n \nu_j k_j(s) \leq L_k^P(s)$, $\forall s \in E$. Since $\boldsymbol{\nu} = \boldsymbol{\nu}^+ - \boldsymbol{\nu}^- = \mathbf{D}\tilde{\boldsymbol{\nu}}$ with $\mathbf{D} = [\mathbf{I}_{n \times n} \quad -\mathbf{I}_{n \times n}]$ and

$$\|\boldsymbol{\nu}\|_1^l = \sum_{j=1}^n l_j |\nu_j| \leq \sum_{j=1}^n l_j (\nu_j^+ + \nu_j^-) = \tilde{\mathbf{l}}^T \tilde{\boldsymbol{\nu}}, \quad \text{with} \quad \tilde{\mathbf{l}} = \begin{bmatrix} \mathbf{l} \\ \mathbf{l} \end{bmatrix}, \quad (31)$$

any feasible point of the linear program

$$\begin{aligned} &\sup_{\tilde{\boldsymbol{\nu}} \in \mathbb{R}^{2n}} (\mathbf{D}^T \tilde{\mathbf{g}} - \tilde{\mathbf{l}})^T \tilde{\boldsymbol{\nu}} \\ &\text{subject to} \quad \mathbf{A}\tilde{\boldsymbol{\nu}} \leq \mathbf{b}_k^P, \\ &\quad \quad \quad \tilde{\boldsymbol{\nu}} \geq \mathbf{0}, \end{aligned}$$

yields a conservative lower bound for k th element of $\boldsymbol{\lambda}$ subject to the positivity constraint (P). Similarly, any feasible point of the linear program

$$\begin{aligned} \inf_{\tilde{\boldsymbol{\nu}} \in \mathbb{R}^{2n}} \quad & -(\boldsymbol{D}^T \tilde{\boldsymbol{y}} - \tilde{\boldsymbol{l}})^T \tilde{\boldsymbol{\nu}} \\ \text{subject to} \quad & \boldsymbol{A} \tilde{\boldsymbol{\nu}} \leq -\boldsymbol{b}_k^P, \\ & \tilde{\boldsymbol{\nu}} \geq \mathbf{0}, \end{aligned}$$

is a conservative upper bound.

Similar approach allows us to discretize the monotonicity constraint (D) and the convexity constraint (C). Deriving these constraints is somewhat more complicated, though: for (D), we use a first-order Taylor expansion of the kernels k_j , and for (C) we use a second-order Taylor expansion. For (D), the discretized dual is again a linear program, while for (C) the discretized dual involves optimizing a linear objective function subject to a finite set of nonlinear constraints. Details of the discretizations of (D) and (C) are in Appendix B.

4 Simulation study

4.1 Experiment setup

We demonstrate the shape-constrained strict bounds using a simulation study designed to mimic unfolding the inclusive jet transverse momentum spectrum (CMS Collaboration, 2011, 2013b) in the Compact Muon Solenoid (CMS) experiment (CMS Collaboration, 2008) at the LHC. A jet consists of a collimated stream of energetic particles and is the experimental signature of a quark or a gluon created in the proton-proton collisions at the LHC. The jet transverse momentum spectrum describes the average number of jets as a function of their transverse momentum p_T , that is, their momentum in the direction perpendicular to the proton beam. The transverse momentum is measured in units of electron volts (eV). Measuring the jet p_T spectrum is an important test of the Standard Model of particle physics and can be used to constrain free parameters in the theory.

We simulate the data using the particle-level intensity function

$$f_0(p_T) = L N_0 \left(\frac{p_T}{\text{GeV}} \right)^{-\alpha} \left(1 - \frac{2}{\sqrt{s}} p_T \right)^{\beta} e^{-\gamma/p_T}, \quad 0 < p_T \leq \frac{\sqrt{s}}{2}. \quad (32)$$

Here $L > 0$ is the integrated luminosity (a measure of the amount of collisions produced in the accelerator, measured in units of inverse barns, b^{-1}), \sqrt{s} is the center-of-mass energy of the proton-proton collisions and N_0 , α , β , and γ are positive parameters. This parameterization is motivated by physical considerations and was used in early inclusive jet analyses at the LHC (CMS Collaboration, 2011).

When the jets are reconstructed using calorimeter information, the smearing can be modeled as additive Gaussian noise with zero mean and variance $\sigma(p_T)^2$ satisfying

$$\left(\frac{\sigma(p_T)}{p_T}\right)^2 = \left(\frac{N}{p_T}\right)^2 + \left(\frac{S}{\sqrt{p_T}}\right)^2 + C^2, \quad (33)$$

where N , S and C are fixed positive constants (CMS Collaboration, 2010). Let p'_T denote the smeared transverse momentum. The smeared intensity function is the convolution

$$g_0(p'_T) = \int_E N(p'_T - p_T | 0, \sigma(p_T)^2) f_0(p_T) dp_T, \quad p'_T \in F, \quad (34)$$

and the unfolding problem becomes a heteroscedastic deconvolution problem for Poisson point process observations with the forward kernel given by $k(p'_T, p_T) = N(p'_T - p_T | 0, \sigma(p_T)^2)$.

At the center-of-mass energy $\sqrt{s} = 7$ TeV and in the central part of the CMS detector, realistic values for the parameters of $f_0(p_T)$ are given by $N_0 = 10^{17}$ fb/GeV, $\alpha = 5$, $\beta = 10$ and $\gamma = 10$ GeV and for the parameters of $\sigma(p_T)$ by $N = 1$ GeV, $S = 1$ GeV $^{1/2}$ and $C = 0.05$ (M. Voutilainen, personal communication, 2012). We furthermore set $L = 5.1$ fb $^{-1}$, which corresponds to the size of the CMS 7 TeV dataset.

The true intensity f_0 obviously always satisfies the positivity constraint (P). For the parameter values in our simulations, it is decreasing for $p_T \gtrsim 2.0$ and convex for $p_T \gtrsim 2.8$. In other words, for intermediate and large p_T values, which are the main focus in inclusive jet analyses (CMS Collaboration, 2013b), the true intensity satisfies the monotonicity constraint (D) and the convexity constraint (C). In general, physical considerations lead one to expect the p_T spectrum to satisfy these constraints, at least for intermediate p_T values.

In the simulations that follow, the true and smeared spaces are $E = F = [400 \text{ GeV}, 1000 \text{ GeV}]$ and we divide both spaces into $n = p = 30$ equal-width bins. The dual constraints are discretized using $m + 1 = 10p + 1$ uniformly spaced grid points. This corresponds to subdividing each true bin into 10 sub-bins. All the experiments were implemented in MATLAB using the Optimization Toolbox (Mathworks, 2014). Appendix C gives more implementation details.

4.2 Results

4.2.1 Shape-constrained strict bounds

Figure 3 shows the true intensity f_0 and the unfolded 95 % strict bounds for the different shape constraints. The true value of λ is shown by the horizontal lines. Results are plotted on both linear and logarithmic scales

and the binned quantities are converted to the intensity scale by dividing them by the bin width. The strict bounds confidence intervals cover the true value of λ in every bin. The shape constraints have a marked influence on the interval lengths. Due to the ill-posedness of the problem, the positivity constrained intervals are fairly wide, with zero lower bound in every bin (these intervals are still orders of magnitude shorter than unconstrained intervals). But with the stronger monotonicity and convexity constraints, the intervals become much shorter and more powerful for making physical inferences.

Figure 4 shows the dual constraints $\pm L_{10}^P$, $\pm L_{10}^D$ and $\pm L_{10}^C$ (see Section 3.3) and the corresponding optimal solutions at the 10th true bin. Despite the conservative discretization, the optimal solutions can be very close to the constraints and hence the conservative discretization is not too restrictive. For the positive lower bound, the optimal solution is $\tilde{\nu} = \mathbf{0}$, which is consistent with the lower bound $\underline{\lambda}_{10} = 0$.

By construction, the joint coverage probability of the strict bounds in Figure 3 is at least 95 %, but in practice it can be much greater than this. To study the actual coverage probability, we repeated the study for 1 000 independent realizations of the data-generating process. For every realization, the intervals covered the actual value of λ : in this example, the joint coverage probability is very close to 100 % (the 95 % Clopper–Pearson confidence interval for the coverage probability is [0.996, 1.000]).

4.2.2 Undercoverage of existing methods

Currently, the two most commonly used unfolding methods in LHC data analysis are the SVD variant of Tikhonov regularization (Höcker and Kartvelishvili, 1996) and the EM iteration with early stopping (D’Agostini, 1995), typically called *D’Agostini iteration* in the high energy physics literature. As explained in Section 1, these estimators are regularized by biasing the solution towards a Monte Carlo prediction λ^{MC} of the quantity of interest λ . The continuous forward mapping is also discretized using the Monte Carlo event generator. When the Monte Carlo prediction differs from the truth, which in practice is always the case, the currently used standard error intervals, which only account for the variance of $\hat{\lambda}$ and not for the bias, can suffer from major undercoverage. This section demonstrates the severity of the problem by unfolding the inclusive jet p_T spectrum with the SVD and D’Agostini methods.

We assume that the Monte Carlo event generator predicts a spectrum that is a slight perturbation of the true f_0 . More specifically, we assume that the Monte Carlo spectrum f^{MC} is given by Equation (32), with the parameters $N_0 = 5.5 \cdot 10^{19}$ fb/GeV, $\alpha = 6$ and $\beta = 12$. The rest of the parameters are set to the same values listed above. This spectrum falls off slightly faster than f_0 in both the power-law and the energy cutoff terms.

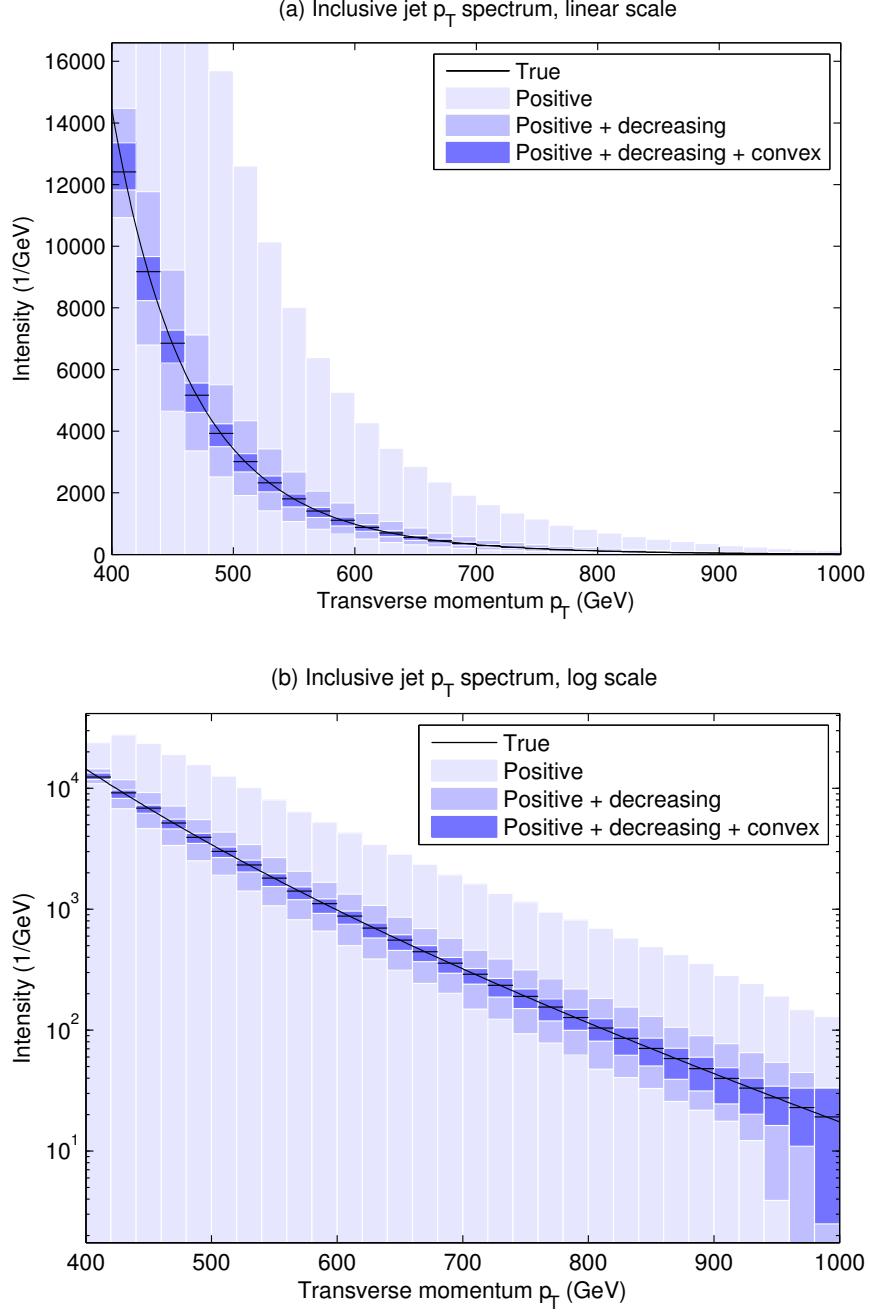


Figure 3: Shape-constrained strict bounds for the inclusive jet transverse momentum spectrum. Figure (a) shows the results on the linear scale and Figure (b) on the logarithmic scale. These intervals are guaranteed to have 95 % joint finite-sample coverage, and indeed do cover the truth across the whole spectrum.

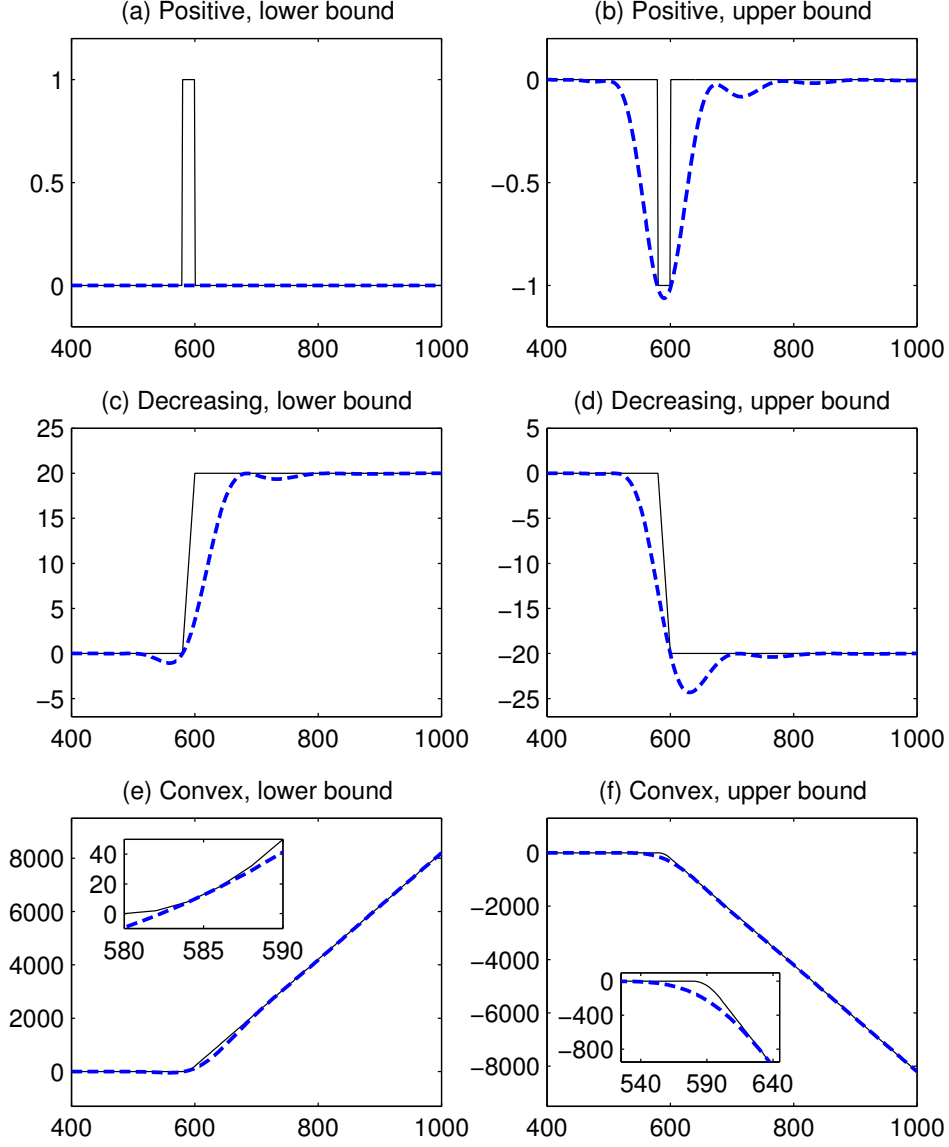


Figure 4: The dual constraints $\pm L_{10}^P$, $\pm L_{10}^D$ and $\pm L_{10}^C$ (solid lines) and the optimal solutions (dashed lines) for the 10th true bin, for the various shape constraints. The insets in Figures (e) and (f) show the quadratic part of the constraint in greater detail.

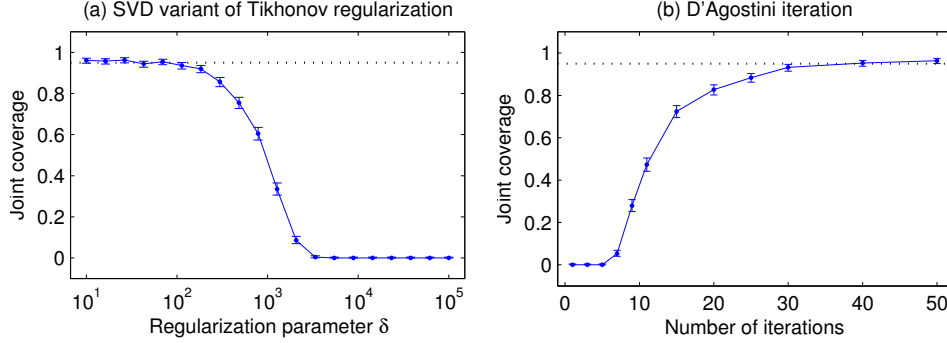


Figure 5: Empirical joint coverage of Bonferroni-corrected 95 % standard error intervals with (a) the SVD variant of Tikhonov regularization and (b) the D’Agostini iteration. The error bars are given by the 95 % Clopper–Pearson intervals and the nominal confidence level is shown by the dotted line. When the regularization is strong, both methods have gross undercoverage.

The value of N_0 is chosen so that the overall scale of f^{MC} is similar to the true f_0 and has little to no impact on the results (it cancels out in SVD unfolding). The discretized smearing matrix \mathbf{K} and the MC prediction $\boldsymbol{\lambda}^{\text{MC}}$ are then obtained by substituting f^{MC} into Equations (4) and (10).

We quantify the uncertainty of each component of $\hat{\boldsymbol{\lambda}}$ using the $1 - \alpha$ standard error intervals

$$\left[\hat{\lambda}_k - z_{1-\alpha/2} \sqrt{\widehat{\text{Var}}(\hat{\lambda}_k)}, \hat{\lambda}_k + z_{1-\alpha/2} \sqrt{\widehat{\text{Var}}(\hat{\lambda}_k)} \right], \quad k = 1, \dots, p, \quad (35)$$

where $z_{1-\alpha/2}$ is the $1 - \alpha/2$ standard normal quantile and $\widehat{\text{Var}}(\hat{\lambda}_k)$ is the estimated variance of $\hat{\lambda}_k$. This follows the approach currently implemented for uncertainty quantification in standard unfolding software (Adye, 2011; Schmitt, 2012), where the uncertainties are typically calculated at 68 % confidence level with $z_{1-\alpha/2} = 1$. To obtain joint confidence sets for the whole histogram $\boldsymbol{\lambda}$, we apply a Bonferroni correction to the binwise intervals. In both the SVD and D’Agostini methods, the variances $\widehat{\text{Var}}(\hat{\lambda}_k)$ are estimated using error propagation; for details, see Appendix C, which also provides a detailed description of the two methods.

The coverage properties of the standard error intervals of Equation (35) depend strongly on the regularization strength, which, in the case of Tikhonov regularization, is controlled by the regularization parameter δ (see Equation (5)) and, in the case of the D’Agostini method, by the number of iterations. Figure 5 shows the joint coverage of 95 % Bonferroni-corrected standard error intervals as a function of the regularization strength for 1 000 independent replications. For weak regularization, the intervals attain their nominal coverage, but for strong regularization, the joint coverage quickly drops to zero.

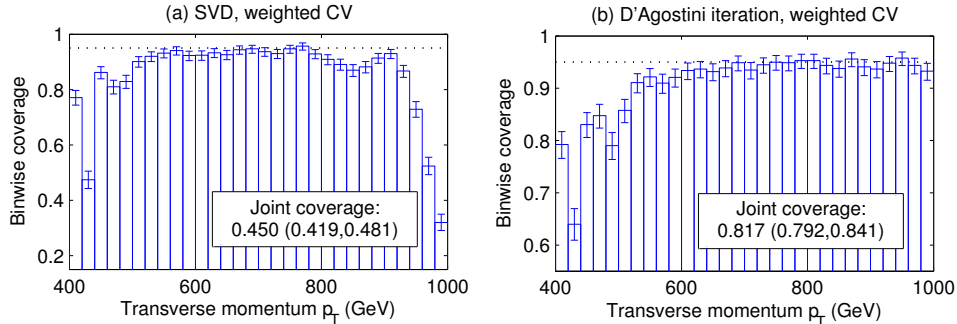


Figure 6: Empirical coverage of the 95 % standard error intervals with (a) the SVD variant of Tikhonov regularization and (b) the D’Agostini iteration, when the regularization strength is chosen using weighted cross-validation. The joint coverage is given for Bonferroni-corrected intervals. The uncertainties are the 95 % Clopper–Pearson intervals for the coverage probability. The nominal confidence level is shown by the dotted line. Both methods have undercoverage at small p_T values and SVD also at large p_T . In both cases, the joint coverage is below the nominal value of 95 %, with SVD in particular having dramatic undercoverage.

An obvious question to ask is where along these coverage curves do typical unfolding results lie? Unfortunately, it is impossible to tell: it depends on how good the Monte Carlo predictions f^{MC} are and how the regularization strength is chosen. Currently, most analyses use nonstandard heuristics for choosing the regularization strength, without properly documenting and justifying the criterion used. For instance, in the case of the D’Agostini iteration, ROOUNFOLD documentation (Adye, 2011) recommends using four iterations, and many LHC analyses seem to follow this convention. Of course, there is no principled reason to use four iterations, and, for example in our particular case, this would lead to the catastrophic result of zero joint coverage.

Even if a more principled, data-driven criterion were used, appropriate coverage performance is far from guaranteed. Figure 6 shows binwise and joint empirical coverages of the two methods for 1 000 independent replications when the regularization strength is chosen using weighted cross-validation (see Appendix C for details; for D’Agostini, 3 runs where the cross-validation score was still decreasing after 20 000 iterations were discarded from the analysis). All the results are for 95 % nominal confidence. Both methods undercover for small p_T values and the SVD approach also undercovers at large p_T values. For SVD, the smallest binwise coverage is only 0.320 (0.291, 0.349) (95 % Clopper–Pearson interval) and for D’Agostini 0.638 (0.607, 0.668), much less than the nominal 0.95. Obviously, when f^{MC} is further away from the true f_0 , one can easily obtain even worse coverage results. We also experimented with adding Monte Carlo noise to λ^{MC} , which

led to a further, large reduction in the coverage.

Caution should be exercised in extrapolating these findings to current LHC unfolding results. The current practice treats the Monte Carlo model dependence as a systematic uncertainty. A typical way to take this uncertainty into account is to compute the unfolded histograms using two or more Monte Carlo event generators and to take the observed differences as an estimate of the systematic uncertainty. The success of this approach obviously depends on how well the Monte Carlo models represent the space of plausible truths and on whether the true f_0 is in some sense “bracketed” by the models.

Clearly, the coverage of existing unfolding methods is a delicate function of the Monte Carlo prediction f^{MC} , the number of true bins p , the regularization method, the regularization strength, and the way these factors are taken into account as systematic uncertainties. It is possible that the coverage is close to the nominal value, but it would require many fortuitous accidents. It seems very difficult, if not impossible, to give rigorous coverage guarantees for the existing methods. In contrast, shape-constrained strict bounds do not rely on a Monte Carlo prediction of the unknown and do not require the analyst to choose a regularization strength. Moreover, the bounds are guaranteed to have nominal joint coverage for any number of true bins p provided f_0 satisfies the given shape constraints, a safe assumption for typical steeply falling spectra.

5 Discussion

We have presented a novel approach for unfolding elementary particle spectra that imposes physically motivated shape constraints and quantifies the uncertainty of the solution using *strict bounds*. To the best of our knowledge, this is the first method that provides guaranteed frequentist coverage in this problem, provided the shape constraints hold. The constraints we have considered hold for an important class of unfolding problems with steeply falling spectra. For other classes of problems, other types of shape constraints, such as unimodality, might still provide an attractive way to reduce uncertainty. A natural direction for future work would hence be to extend the approach presented here to k -modal intensities (Hengartner and Stark, 1995).

The type of coverage considered in this work, namely joint coverage for the whole histogram λ , differs from the binwise coverage traditionally considered in high energy physics. Binwise confidence intervals can be used to make inferential statements at a single bin, but—due to inevitable correlations between the bins—interpreting the collection of such intervals as a whole is difficult. This issue has been noted in the high energy physics literature (Blobel, 2013, Section 6.6.4). In contrast, joint confidence intervals, such as those in Figure 3(a), by definition have the property that, under re-

peated sampling, at least 95 % of the envelopes formed by the intervals will contain the entire true histogram λ . Hence, joint intervals can be directly interpreted as a whole, making them more useful than binwise intervals. For example, the envelope formed by the 95 % joint intervals yields a goodness-of-fit test of a theory prediction of λ with Type I error probability not larger than 5 %.

An important limitation of the present work is it assumes perfect knowledge of the smearing kernel $k(t, s)$, which in practice is usually determined using some auxiliary measurements or simulations, and hence is uncertain. If rigorous uncertainty quantification for $k(t, s)$ is available, it is possible to incorporate these uncertainties into the strict bounds construction (Stark, 1992, Section 9.2). We expect this to be feasible at least when there is a physics-driven parametric model for $k(t, s)$, such as the calorimeter response in Equation (34). Rigorous treatment of the nonparametric case, where estimating $k(t, s)$ essentially becomes a nonparametric quantile regression problem, appears significantly harder. Of course, these considerations also affect existing unfolding methods, where the uncertainty of the smearing kernel is typically taken into account as a systematic uncertainty estimated using various heuristics.

The new method potentially has large overcoverage: the intervals may be wider than necessary. The most important sources of slack are the choice of Ξ (Stark, 1992, Section 10.2) and the projection of $C \cap D$ into the finite-dimensional set $[\underline{\lambda}_1, \bar{\lambda}_1] \times \cdots \times [\underline{\lambda}_p, \bar{\lambda}_p]$ (see Section 2). Selecting Ξ optimally is an open problem.

Acknowledgments

We warmly thank Victor Panaretos for his support of this work. We are also grateful to Olaf Behnke, Bob Cousins, Tommaso Dorigo, Louis Lyons, Igor Volobouev and Mikko Voutilainen for helpful discussions and to Yoav Zemel for insightful feedback on the manuscript. Parts of this work were carried out while MK was visiting the Department of Statistics at the University of California, Berkeley.

A Derivation of the dual constraints for decreasing and convex intensities

This section writes the constraint $\int_E h_k(s) f(s) ds \geq 0, \forall f \in C$, in an equivalent form that does not involve f . Clearly, in the case of the positivity constraint (P), an equivalent constraint is $h_k(s) \geq 0, \forall s \in E$. The derivations for the monotonicity constraint (D) and the convexity constraint (C) employ integration by parts.

A.1 Decreasing intensities

We shall show that, when C is the monotonicity constraint (D),

$$\int_E h_k(s) f(s) ds \geq 0, \forall f \in C \Leftrightarrow \int_{E_{\min}}^s h_k(s') ds' \geq 0, \forall s \in E. \quad (36)$$

Integration by parts yields

$$\begin{aligned} \int_E h_k(s) f(s) ds &= \int_{E_{\min}}^s h_k(s') ds' f(s) \Big|_{E_{\min}}^{E_{\max}} - \int_E \int_{E_{\min}}^s h_k(s') ds' f'(s) ds \\ &= \int_E h_k(s) ds f(E_{\max}) - \int_E \int_{E_{\min}}^s h_k(s') ds' f'(s) ds. \end{aligned} \quad (37)$$

From this, it is clear that the right-hand side of Equation (36) implies the left-hand side. To show the opposite direction, let us assume that $\int_{E_{\min}}^{s^*} h_k(s') ds' < 0$ for some s^* in the interior of E . Then by the continuity of the integral, $\int_{E_{\min}}^s h_k(s') ds' < 0$ for all $s \in (s^* - \delta, s^* + \delta)$ for some $\delta > 0$. Consider a function $d \in C$ that is a strictly positive constant on the interval $[E_{\min}, s^* - \delta]$ and zero on $[s^* + \delta, E_{\max}]$. Substituting d into Equation (37) gives

$$\int_E h_k(s) d(s) ds = - \int_{s^* - \delta}^{s^* + \delta} \int_{E_{\min}}^s h_k(s') ds' d'(s) ds < 0, \quad (38)$$

a contradiction. Hence $\int_{E_{\min}}^s h_k(s') ds' \geq 0$ for all s in the interior of E and, by continuity, for all $s \in E$.

A.2 Convex intensities

We next address the convexity constraint (C) by showing that

$$\begin{aligned} \int_E h_k(s) f(s) ds &\geq 0, \forall f \in C \\ \Leftrightarrow \int_{E_{\min}}^s \int_{E_{\min}}^{s'} h_k(s'') ds'' ds' &\geq 0, \forall s \in E \quad \wedge \quad \int_E h_k(s) ds \geq 0. \end{aligned} \quad (39)$$

Integrating Equation (37) by parts twice gives

$$\begin{aligned} \int_E h_k(s) f(s) ds &= \int_E h_k(s) ds f(E_{\max}) - \int_{E_{\min}}^s \int_{E_{\min}}^{s'} h_k(s'') ds'' ds' f'(s) \Big|_{E_{\min}}^{E_{\max}} \\ &\quad + \int_E \int_{E_{\min}}^s \int_{E_{\min}}^{s'} h_k(s'') ds'' ds' f''(s) ds \\ &= \int_E h_k(s) ds f(E_{\max}) - \int_{E_{\min}}^{E_{\max}} \int_{E_{\min}}^s h_k(s') ds' ds f'(E_{\max}) \\ &\quad + \int_E \int_{E_{\min}}^s \int_{E_{\min}}^{s'} h_k(s'') ds'' ds' f''(s) ds. \end{aligned} \quad (40)$$

From this form one can see that the right-hand side of Equation (39) implies the left-hand side. To show the reverse implication, pick $d \in C$ such that $d(s) = a > 0$ for all $s \in E$. Substituting this into the left-hand side implies that $\int_E h_k(s) ds \geq 0$. Let us next assume that $\int_{E_{\min}}^{s^*} \int_{E_{\min}}^{s'} h_k(s'') ds'' ds' < 0$ for some s^* in the interior of E . By the continuity of the integral, it follows that $\int_{E_{\min}}^s \int_{E_{\min}}^{s'} h_k(s'') ds'' ds' < 0$ for all $s \in (s^* - \delta, s^* + \delta)$ for some $\delta > 0$. Consider a function $d \in C$ that is linear and strictly decreasing on the interval $[E_{\min}, s^* - \delta]$ and zero on $[s^* + \delta, E_{\max}]$. Substituting d into Equation (40) yields

$$\int_E h_k(s) d(s) ds = \int_{s^* - \delta}^{s^* + \delta} \int_{E_{\min}}^s \int_{E_{\min}}^{s'} h_k(s'') ds'' ds' d(s) ds < 0, \quad (41)$$

a contradiction. Hence $\int_{E_{\min}}^s \int_{E_{\min}}^{s'} h_k(s'') ds'' ds' \geq 0$ for all s in the interior of E and, by continuity, for all $s \in E$.

B Discretized constraints for decreasing and convex intensities

This section derives conservative discretizations of the dual constraints for the monotonicity constraint (D) and the convexity constraint (C). The strategy follows the procedure of Section 3.4, with appropriate modifications. Discretizing the constraints $\sum_{j=1}^n \nu_j k_j^*(s) \leq \pm L_k^D(s)$ or $\sum_{j=1}^n \nu_j k_j^{**}(s) \leq \pm L_k^C(s)$ by applying the bound of Equation (28) to k_j^* or k_j^{**} gives up too much because Equation (28) bounds the left-hand side by a constant on each interval $[s_i, s_{i+1})$, while the functions $\pm L_k^D$ or $\pm L_k^C$ on the right-hand side can vary within these intervals. A better approach for the monotonicity constraint (D) is to use a first-order Taylor expansion of k_j^* , which gives a linear upper bound for the left-hand side. For the convexity constraint (C), we use a second-order Taylor expansion of k_j^{**} , which yields a quadratic upper bound.

B.1 Decreasing intensities

Let us first address the monotonicity constraint (D). For any $s \in [s_i, s_{i+1})$,

$$\begin{aligned} k_j^*(s) &= k_j^*(s_i) + (k_j^*)'(\xi_j)(s - s_i) \\ &= k_j^*(s_i) + k_j(\xi_j)(s - s_i), \quad \xi_j \in [s_i, s). \end{aligned} \quad (42)$$

This yields

$$\begin{aligned}
\sum_{j=1}^n \nu_j k_j^*(s) &= \sum_{j=1}^n \nu_j k_j^*(s_i) + \sum_{j=1}^n \nu_j^+ k_j(\xi_j)(s - s_i) - \sum_{j=1}^n \nu_j^- k_j(\xi_j)(s - s_i) \\
&\leq \sum_{j=1}^n \nu_j k_j^*(s_i) + \sum_{j=1}^n \nu_j^+ \sup_{\xi \in [s_i, s_{i+1})} k_j(\xi)(s - s_i) \\
&\quad - \sum_{j=1}^n \nu_j^- \inf_{\xi \in [s_i, s_{i+1})} k_j(\xi)(s - s_i) \\
&= \sum_{j=1}^n \nu_j k_j^*(s_i) + \sum_{j=1}^n \nu_j^+ \bar{\rho}_{i,j}(s - s_i) - \sum_{j=1}^n \nu_j^- \underline{\rho}_{i,j}(s - s_i). \quad (43)
\end{aligned}$$

On $[s_i, s_{i+1})$, this gives a linear upper bound for $\sum_{j=1}^n \nu_j k_j^*(s)$. Since L_k^D is linear on each interval $[s_i, s_{i+1})$, it is enough to enforce the constraint at the endpoints of the interval. By the continuity of L_k^D , we require for each $i = 1, \dots, m$ that

$$\begin{cases} \sum_{j=1}^n \nu_j k_j^*(s_i) \leq \pm L_k^D(s_i), \\ \sum_{j=1}^n \nu_j k_j^*(s_i) + \sum_{j=1}^n \nu_j^+ \bar{\rho}_{i,j} \delta_i - \sum_{j=1}^n \nu_j^- \underline{\rho}_{i,j} \delta_i \leq \pm L_k^D(s_{i+1}), \end{cases} \quad (44)$$

where $\delta_i = s_{i+1} - s_i$. In fact, since $\sum_{j=1}^n \nu_j k_j^*(s)$ is continuous, the first inequality in Equation (44) is redundant: it suffices to enforce the second.

Let $\mathbf{\Delta} \equiv \text{diag}(\{\delta_i\}_{i=1}^m)$; let \mathbf{K}^* denote the matrix with elements $K_{i,j}^* = k_j^*(s_i)$, $i = 1, \dots, m$, $j = 1, \dots, n$; and let \mathbf{b}_k^D denote the vector with elements $b_{k,i}^D = L_k^D(s_{i+1})$, $i = 1, \dots, m$. Then $(\mathbf{K}^* \mathbf{D} + \mathbf{\Delta} \mathbf{A}) \tilde{\mathbf{v}} \leq \pm \mathbf{b}_k^D$ is a conservative discretization of the constraint $\sum_{j=1}^n \nu_j k_j^*(s) \leq \pm L_k^D(s)$, $\forall s \in E$, where the matrices \mathbf{A} and \mathbf{D} are defined in Section 3.4.

To summarize, any feasible point of the linear program

$$\begin{aligned} & \sup_{\tilde{\mathbf{v}} \in \mathbb{R}^{2n}} (\mathbf{D}^T \tilde{\mathbf{g}} - \tilde{\mathbf{l}})^T \tilde{\mathbf{v}} \\ \text{subject to } & (\mathbf{K}^* \mathbf{D} + \mathbf{\Delta} \mathbf{A}) \tilde{\mathbf{v}} \leq \mathbf{b}_k^D, \\ & \tilde{\mathbf{v}} \geq \mathbf{0} \end{aligned}$$

yields a conservative lower bound at the k th true bin. A conservative upper bound is given by any feasible point of

$$\begin{aligned} & \inf_{\tilde{\mathbf{v}} \in \mathbb{R}^{2n}} -(\mathbf{D}^T \tilde{\mathbf{g}} - \tilde{\mathbf{l}})^T \tilde{\mathbf{v}} \\ \text{subject to } & (\mathbf{K}^* \mathbf{D} + \mathbf{\Delta} \mathbf{A}) \tilde{\mathbf{v}} \leq -\mathbf{b}_k^D, \\ & \tilde{\mathbf{v}} \geq \mathbf{0}. \end{aligned}$$

B.2 Convex intensities

Let us then focus on the convexity constraint (C). For any $s \in [s_i, s_{i+1})$,

$$k_j^{**}(s) = k_j^{**}(s_i) + (k_j^{**})'(s_i)(s - s_i) + \frac{1}{2}(k_j^{**})''(\xi_j)(s - s_i)^2 \quad (45)$$

$$= k_j^{**}(s_i) + k_j^*(s_i)(s - s_i) + \frac{1}{2}k_j(\xi_j)(s - s_i)^2, \quad \xi_j \in [s_i, s). \quad (46)$$

This yields

$$\begin{aligned} \sum_{j=1}^n \nu_j k_j^{**}(s) &= \sum_{j=1}^n \nu_j k_j^{**}(s_i) + \sum_{j=1}^n \nu_j k_j^*(s_i)(s - s_i) + \frac{1}{2} \sum_{j=1}^n \nu_j k_j(\xi_j)(s - s_i)^2 \\ &\leq \sum_{j=1}^n \nu_j k_j^{**}(s_i) + \sum_{j=1}^n \nu_j k_j^*(s_i)(s - s_i) \\ &\quad + \frac{1}{2} \sum_{j=1}^n \left(\nu_j^+ \bar{\rho}_{i,j} - \nu_j^- \underline{\rho}_{i,j} \right) (s - s_i)^2, \end{aligned} \quad (47)$$

where the bound is established as in Equation (43). This bounds $\sum_{j=1}^n \nu_j k_j^{**}(s)$ on $[s_i, s_{i+1})$ from above by a parabola. If we ensure that this parabola lies below $\pm L_k^C$ for every $s \in [s_i, s_{i+1})$, the resulting feasible set is a subset of the original constraint set that involved infinitely many constraints. We need to require that

$$\pm L_k^C(s) - \sum_{j=1}^n \nu_j k_j^{**}(s_i) - \sum_{j=1}^n \nu_j k_j^*(s_i)(s - s_i) \quad (48)$$

$$- \frac{1}{2} \sum_{j=1}^n \left(\nu_j^+ \bar{\rho}_{i,j} - \nu_j^- \underline{\rho}_{i,j} \right) (s - s_i)^2 \geq 0, \quad \forall s \in [s_i, s_{i+1}). \quad (49)$$

Since L_k^C is either linear or quadratic on $[s_i, s_{i+1})$, the left-hand side is a parabola. We need to ensure that this parabola is positive on the interval $[s_i, s_{i+1})$. Let $a_{i,k}s^2 + b_{i,k}s + c_{i,k}$ be the parabola corresponding to the left-hand side and let $s_{i,k}^* = -b_{i,k}/(2a_{i,k})$ be the s -coordinate of its vertex. Then $a_{i,k}s^2 + b_{i,k}s + c_{i,k} \geq 0, \forall s \in [s_i, s_{i+1})$, is equivalent to requiring that

$$\begin{cases} a_{i,k}s_i^2 + b_{i,k}s_i + c_{i,k} \geq 0, \\ a_{i,k}s_{i+1}^2 + b_{i,k}s_{i+1} + c_{i,k} \geq 0, \\ \mathbf{1}_{(s_i, s_{i+1})}(s_{i,k}^*)(a_{i,k}(s_{i,k}^*)^2 + b_{i,k}s_{i,k}^* + c_{i,k}) \geq 0. \end{cases} \quad (50)$$

The first two conditions guarantee that the end points of the parabola lie above the s -axis, while the last condition ensures that the vertex is above the s -axis if it is located on the interval (s_i, s_{i+1}) . As before, by the continuity

of $\sum_{j=1}^n \nu_j k_j^{**}(s)$ and $L_k^C(s)$, the first condition is redundant and can be dropped.

Here $s_{i,k}^*$ depends nonlinearly on $\tilde{\nu}$, so the conservatively discretized optimization problem is not a linear program. Nevertheless, a conservative lower bound at the k th true bin can be found by solving

$$\begin{aligned} & \sup_{\tilde{\nu} \in \mathbb{R}^{2n}} (\mathbf{D}^T \tilde{\mathbf{y}} - \tilde{\mathbf{l}})^T \tilde{\nu} \\ \text{subject to } & a_{i,k} s_{i+1}^2 + b_{i,k} s_{i+1} + c_{i,k} \geq 0, \quad i = 1, \dots, m, \\ & \mathbf{1}_{(s_i, s_{i+1})}(s_{i,k}^*)(a_{i,k}(s_{i,k}^*)^2 + b_{i,k}s_{i,k}^* + c_{i,k}) \geq 0, \quad i = 1, \dots, m, \\ & - \sum_{j=1}^n (\nu_j^+ - \nu_j^-) k_j^*(E_{\max}) \geq E_{k,\min} - E_{k,\max}, \\ & \tilde{\nu} \geq \mathbf{0}, \end{aligned}$$

where $\tilde{\nu} = \begin{bmatrix} \nu^+ \\ \nu^- \end{bmatrix}$, $s_{i,k}^* = -\frac{b_{i,k}}{2a_{i,k}}$ and the coefficients $a_{i,k}$, $b_{i,k}$ and $c_{i,k}$, which depend on $\tilde{\nu}$, are given by

$$a_{i,k} = \begin{cases} -A_i, & s_i < E_{k,\min}, \\ -A_i + \frac{1}{2}, & E_{k,\min} \leq s_i < E_{k,\max}, \\ -A_i, & s_i \geq E_{k,\max}, \end{cases} \quad (51)$$

$$b_{i,k} = \begin{cases} 2A_i s_i - B_i, & s_i < E_{k,\min}, \\ 2A_i s_i - B_i - E_{k,\min}, & E_{k,\min} \leq s_i < E_{k,\max}, \\ 2A_i s_i - B_i + E_{k,\max} - E_{k,\min}, & s_i \geq E_{k,\max}, \end{cases} \quad (52)$$

$$c_{i,k} = \begin{cases} -A_i s_i^2 + B_i s_i - C_i, & s_i < E_{k,\min}, \\ -A_i s_i^2 + B_i s_i - C_i + \frac{1}{2} E_{k,\min}^2, & E_{k,\min} \leq s_i < E_{k,\max}, \\ -A_i s_i^2 + B_i s_i - C_i - \frac{1}{2} E_{k,\max}^2 + \frac{1}{2} E_{k,\min}^2, & s_i \geq E_{k,\max}, \end{cases} \quad (53)$$

where

$$A_i = \frac{1}{2} \sum_{j=1}^n (\nu_j^+ \bar{\rho}_{i,j} - \nu_j^- \underline{\rho}_{i,j}), \quad (54)$$

$$B_i = \sum_{j=1}^n (\nu_j^+ - \nu_j^-) k_j^*(s_i), \quad (55)$$

$$C_i = \sum_{j=1}^n (\nu_j^+ - \nu_j^-) k_j^{**}(s_i). \quad (56)$$

Similarly, the corresponding upper bound is given by the solution of

$$\begin{aligned}
& \inf_{\tilde{\nu} \in \mathbb{R}^{2n}} && -(\mathbf{D}^T \tilde{\mathbf{y}} - \tilde{\mathbf{l}})^T \tilde{\nu} \\
\text{subject to} &&& a_{i,k} s_{i+1}^2 + b_{i,k} s_{i+1} + c_{i,k} \geq 0, \quad i = 1, \dots, m, \\
&&& \mathbf{1}_{(s_i, s_{i+1})}(s_{i,k}^*)(a_{i,k}(s_{i,k}^*)^2 + b_{i,k}s_{i,k}^* + c_{i,k}) \geq 0, \quad i = 1, \dots, m, \\
&&& -\sum_{j=1}^n (\nu_j^+ - \nu_j^-) k_j^*(E_{\max}) \geq E_{k,\max} - E_{k,\min}, \\
&&& \tilde{\nu} \geq \mathbf{0},
\end{aligned}$$

where the coefficients are

$$a_{i,k} = \begin{cases} -A_i, & s_i < E_{k,\min}, \\ -A_i - \frac{1}{2}, & E_{k,\min} \leq s_i < E_{k,\max}, \\ -A_i, & s_i \geq E_{k,\max}, \end{cases} \quad (57)$$

$$b_{i,k} = \begin{cases} 2A_i s_i - B_i, & s_i < E_{k,\min}, \\ 2A_i s_i - B_i + E_{k,\min}, & E_{k,\min} \leq s_i < E_{k,\max}, \\ 2A_i s_i - B_i - E_{k,\max} + E_{k,\min}, & s_i \geq E_{k,\max}, \end{cases} \quad (58)$$

$$c_{i,k} = \begin{cases} -A_i s_i^2 + B_i s_i - C_i, & s_i < E_{k,\min}, \\ -A_i s_i^2 + B_i s_i - C_i - \frac{1}{2} E_{k,\min}^2, & E_{k,\min} \leq s_i < E_{k,\max}, \\ -A_i s_i^2 + B_i s_i - C_i + \frac{1}{2} E_{k,\max}^2 - \frac{1}{2} E_{k,\min}^2, & s_i \geq E_{k,\max} \end{cases} \quad (59)$$

and A_i , B_i and C_i are given by Equations (54)–(56).

These optimization problems can be solved using standard nonlinear programming algorithms, but some care is needed to choose the algorithm and its starting point; see Section C.1. Since any feasible point of these programs yields a conservative bound, we only need to find a good feasible point, not necessarily a global optimum.

C Implementation details

This appendix provides implementation details for the unfolding methods used in this paper. Section C.1 focuses on the shape-constrained strict bounds, while Sections C.2 and C.3 provide a detailed description of our implementation of the SVD and D’Agostini methods, respectively.

C.1 Shape-constrained strict bounds

The optimization problems to find the shape-constrained strict bounds are somewhat challenging to solve because they involve a relatively high-dimensional solution space, numerical values on very different scales, and fairly complicated constraints. As a result, some care is needed in the numerical implementation, including verifying the validity of the output of the optimization algorithms.

For positivity and monotonicity constraints, where the bounds can be found by solving a linear program, we used the interior-point linear program solver implemented in the `linprog` function in the MATLAB Optimization Toolbox (Mathworks, 2014). For the convexity constraint, which requires solving a nonlinear program, we used the sequential quadratic programming (SQP) algorithm as implemented in the `fmincon` function in the MATLAB Optimization Toolbox (Mathworks, 2014).

The optimization problems described in Sections 3.4, B.1, and B.2 tend to be numerically unstable when the solver explores large values of $\tilde{\nu}$. We address this issue by imposing an upper bound on $\tilde{\nu}$. For each j , we replace the constraint $\tilde{\nu}_j \geq 0$ with the constraint $0 \leq \tilde{\nu}_j \leq M$, where M is chosen to be large enough that the upper bound is not active at the optimal solution. (Notice that even if the upper bound were active, the solution still gives a valid confidence bound, because the restricted feasible set is a subset of the original feasible set.) Imposing the upper bound significantly improved the stability of the numerical solvers. For the numerical experiments of this paper, M was set to 30 for the positivity constraint, 15 for the monotonicity constraint, and 10 for the convexity constraint.

The solution found by the optimization algorithms can violate the constraints within a preset numerical tolerance. This infeasibility could make the confidence bound optimistic rather than conservative. To ensure that this does not happen, we verify the feasibility of the optimal solution. If it is infeasible, we iteratively scale ν^+ down and ν^- up until the solution becomes feasible. Typically very little fine-tuning of this kind was required to obtain a feasible point.

The SQP algorithm requires a good feasible starting point. To find one, we first solve the linear program corresponding to the unconservative discretization

$$\sum_{j=1}^n \nu_j k_j^{**}(s_i) \leq \pm L_k^C(s_i), \quad i = 1, \dots, m+1. \quad (60)$$

We then scale the solution as described above to make it feasible for the conservative discretization; the result is then used as the initial feasible point for SQP.

The implementation described here worked fairly robustly for the inclusive jet spectrum of Section 4. Occasionally, the algorithms found a suboptimal feasible point. This maintains conservative confidence, but adjusting the tuning parameters of the optimization algorithms may help identify a better feasible point. For the lower bound, the point $\tilde{\nu} = \mathbf{0}$ is always feasible (yielding a lower bound of zero), while, for the upper bound, the algorithms might find no feasible point, in which case the upper confidence bound is $+\infty$.

C.2 SVD variant of Tikhonov regularization

The SVD unfolding technique of Höcker and Kartvelishvili (1996) can be understood as a variant of Tikhonov regularization where the unfolded estimator $\hat{\boldsymbol{\lambda}}$ in the discretized model $\mathbf{y} \sim \text{Poisson}(\mathbf{K}\boldsymbol{\lambda})$ solves the optimization problem

$$\min_{\boldsymbol{\lambda} \in \mathbb{R}^p} (\mathbf{y} - \mathbf{K}\boldsymbol{\lambda})^\top \hat{\mathbf{C}}^{-1} (\mathbf{y} - \mathbf{K}\boldsymbol{\lambda}) + \delta \|\tilde{\mathbf{L}}\boldsymbol{\lambda}\|_2^2, \quad (61)$$

where $\hat{\mathbf{C}} = \text{diag}(\mathbf{y})$ is the estimated covariance of \mathbf{y} and $\tilde{\mathbf{L}} = \mathbf{L} \text{diag}(\boldsymbol{\lambda}^{\text{MC}})^{-1}$ with

$$\mathbf{L} = \begin{bmatrix} -1 & 1 & & & & \\ 1 & -2 & 1 & & & \\ & 1 & -2 & 1 & & \\ & & \ddots & \ddots & \ddots & \\ & & & 1 & -2 & 1 \\ & & & & 1 & -1 \end{bmatrix}. \quad (62)$$

The matrix \mathbf{L} corresponds to a discretized second derivative with reflexive boundary conditions (Hansen, 2010). In other words, the problem is regularized by penalizing the second derivative of the binwise ratio of the unfolded histogram $\boldsymbol{\lambda}$ and its MC prediction $\boldsymbol{\lambda}^{\text{MC}}$.

The solution to Equation (61) yields the point estimator

$$\hat{\boldsymbol{\lambda}} = \underbrace{(\mathbf{K}^\top \hat{\mathbf{C}}^{-1} \mathbf{K} + \delta \tilde{\mathbf{L}}^\top \tilde{\mathbf{L}})^{-1} \mathbf{K}^\top \hat{\mathbf{C}}^{-1}}_{:=\mathbf{K}^+} \mathbf{y} = \mathbf{K}^+ \mathbf{y}. \quad (63)$$

The corresponding estimate of the smeared histogram $\boldsymbol{\mu}$ is $\hat{\boldsymbol{\mu}} = \mathbf{K}\hat{\boldsymbol{\lambda}} = \mathbf{K}\mathbf{K}^+ \mathbf{y} = \mathbf{H}\mathbf{y}$ with $\mathbf{H} = \mathbf{K}\mathbf{K}^+$. Since the variance of \mathbf{y} varies across the bins, we select the regularization parameter δ using weighted leave-one-out cross-validation (Green and Silverman, 1994, Section 3.5.3) with the weight of each bin given by the inverse of its estimated variance: we choose δ to minimize

$$\text{CV} = \sum_{i=1}^n \frac{(y_i - \hat{\mu}_i^{-i})^2}{y_i} = \sum_{i=1}^n \frac{1}{y_i} \left(\frac{y_i - \hat{\mu}_i}{1 - H_{i,i}} \right)^2, \quad (64)$$

where $\hat{\mu}_i^{-i}$ is the estimate of the i th smeared bin obtained using $\mathbf{y}^{-i} = [y_1, \dots, y_{i-1}, y_{i+1}, \dots, y_n]^\top$ and the second equality follows from the linearity of $\hat{\boldsymbol{\lambda}}$.

An estimate of the covariance of $\hat{\boldsymbol{\lambda}}$ (ignoring the data-dependence of δ and $\hat{\mathbf{C}}$) is $\widehat{\text{Cov}}(\hat{\boldsymbol{\lambda}}) = \mathbf{K}^+ \text{diag}(\mathbf{y})(\mathbf{K}^+)^\top$. If the distribution of $\hat{\boldsymbol{\lambda}}$ is approximately Gaussian, its binwise uncertainties can then be quantified using the standard error intervals of Equation (35) with $\widehat{\text{Var}}(\hat{\lambda}_j) = \widehat{\text{Cov}}(\hat{\boldsymbol{\lambda}})_{j,j}$.

C.3 D’Agostini iteration

The D’Agostini iteration (D’Agostini, 1995) is an EM algorithm (Dempster et al., 1977; Shepp and Vardi, 1982; Vardi et al., 1985) for finding a maximum likelihood solution in the discrete forward model $\mathbf{y} \sim \text{Poisson}(\mathbf{K}\boldsymbol{\lambda})$. Given a starting point $\boldsymbol{\lambda}^{(0)} > \mathbf{0}$, the $(t + 1)$ th step of the iteration is

$$\lambda_j^{(t+1)} = \frac{\lambda_j^{(t)}}{\sum_{i=1}^n K_{i,j}} \sum_{i=1}^n \frac{K_{i,j} y_i}{\sum_{k=1}^p K_{i,k} \lambda_k^{(t)}}.$$

The solution is regularized by stopping the algorithm before it converges to a maximum likelihood estimate. In the ROOUNFOLD implementation (Adye, 2011), the iteration starts at a MC prediction of the unfolded histogram, $\boldsymbol{\lambda}^{(0)} = \boldsymbol{\lambda}^{\text{MC}}$.

We choose the stopping point of the D’Agostini iteration using weighted cross-validation, minimizing Equation (64). Since the point estimate $\hat{\boldsymbol{\lambda}}$ is a nonlinear function of \mathbf{y} , the second equality in Equation (64) no longer holds. As a result, evaluating the CV function requires computing n point estimates, one for each left-out smeared bin, which is computationally demanding.

By using a linearized approximation, we can estimate the covariance of $\boldsymbol{\lambda}^{(t+1)}$ by

$$\widehat{\text{Cov}}(\boldsymbol{\lambda}^{(t+1)}) = \mathbf{J}^{(t+1)} \text{diag}(\mathbf{y}) (\mathbf{J}^{(t+1)})^T, \quad (65)$$

where $\mathbf{J}^{(t+1)}$ is the Jacobian of $\boldsymbol{\lambda}^{(t+1)}$ evaluated at \mathbf{y} . Let $\varepsilon_j \equiv \sum_{i=1}^n K_{i,j}$ and

$$M_{i,j}^{(t)} \equiv \frac{\lambda_j^{(t)}}{\varepsilon_j} \frac{K_{i,j}}{\sum_{k=1}^p K_{i,k} \lambda_k^{(t)}}. \quad (66)$$

Then the elements of the Jacobian are (Adye, 2011)

$$J_{j,i}^{(t+1)} = \frac{\partial \lambda_j^{(t+1)}}{\partial y_i} = M_{i,j}^{(t)} + \frac{\lambda_j^{(t+1)}}{\lambda_j^{(t)}} J_{j,i}^{(t)} - \sum_{k=1}^p \sum_{l=1}^n y_l \frac{\varepsilon_k}{\lambda_k^{(t)}} M_{l,j}^{(t)} M_{l,k}^{(t)} J_{k,i}^{(t)}, \quad (67)$$

with $J_{j,i}^{(0)} = 0$ for all i, j . The estimated variances for Equation (35) are then $\widehat{\text{Var}}(\hat{\lambda}_j) = \widehat{\text{Cov}}(\hat{\boldsymbol{\lambda}})_{j,j} = \widehat{\text{Cov}}(\boldsymbol{\lambda}^{(T)})_{j,j}$, where T is the stopping point. These intervals ignore the data-dependence of T and assume that $\hat{\boldsymbol{\lambda}}$ is approximately Gaussian.

References

Adye, T. (2011). Unfolding algorithms and tests using RooUnfold. In Prosper, H. B. and Lyons, L., editors, *Proceedings of the PHYSTAT 2011 Workshop on Statistical Issues Related to Discovery Claims in Search*

- Experiments and Unfolding*, CERN-2011-006, pages 313–318, CERN, Geneva, Switzerland.
- Antoniadis, A. and Bigot, J. (2006). Poisson inverse problems. *The Annals of Statistics*, 34(5):2132–2158.
- ATLAS Collaboration (2012). Measurement of the transverse momentum distribution of W bosons in pp collisions at $\sqrt{s} = 7$ TeV with the ATLAS detector. *Physical Review D*, 85:012005.
- Backus, G. (1970). Inference from inadequate and inaccurate data, I. *Proceedings of the National Academy of Sciences*, 65(1):1–7.
- Blobel, V. (2013). Unfolding. In Behnke, O., Kröninger, K., Schott, G., and Schörner-Sadenius, T., editors, *Data Analysis in High Energy Physics: A Practical Guide to Statistical Methods*, pages 187–225. Wiley.
- CMS Collaboration (2008). The CMS experiment at the CERN LHC. *Journal of Instrumentation*, 3:S08004.
- CMS Collaboration (2010). Measurement of the inclusive jet cross section in pp collisions at 7 TeV. CMS-PAS-QCD-10-011, available at <http://cds.cern.ch/record/1280682>.
- CMS Collaboration (2011). Measurement of the inclusive jet cross section in pp collisions at $\sqrt{s} = 7$ TeV. *Physical Review Letters*, 107:132001.
- CMS Collaboration (2013a). Measurement of differential top-quark-pair production cross sections in pp collisions at $\sqrt{s} = 7$ TeV. *The European Physical Journal C*, 73:2339.
- CMS Collaboration (2013b). Measurements of differential jet cross sections in proton-proton collisions at $\sqrt{s} = 7$ TeV with the CMS detector. *Physical Review D*, 87:112002.
- CMS Collaboration (2015). Measurement of differential cross sections for Higgs boson production in the diphoton decay channel in pp collisions at $\sqrt{s} = 8$ TeV. Available at <http://arxiv.org/abs/1508.07819>. In press.
- Cowan, G. (1998). *Statistical Data Analysis*. Oxford University Press.
- D’Agostini, G. (1995). A multidimensional unfolding method based on Bayes’ theorem. *Nuclear Instruments and Methods A*, 362:487–498.
- Dempster, A. P., Laird, N. M., and Rubin, D. B. (1977). Maximum likelihood from incomplete data via the EM algorithm. *Journal of the Royal Statistical Society. Series B (Methodological)*, 39(1):1–38.

- Garwood, F. (1936). Fiducial limits for the Poisson distribution. *Biometrika*, 28(3/4):437–442.
- Green, P. J. and Silverman, B. W. (1994). *Nonparametric Regression and Generalized Linear Models: A Roughness Penalty Approach*. Chapman & Hall.
- Hansen, P. C. (2010). *Discrete Inverse Problems: Insight and Algorithms*. SIAM.
- Hengartner, N. W. and Stark, P. B. (1995). Finite-sample confidence envelopes for shape-restricted densities. *The Annals of Statistics*, 23(2):525–550.
- Höcker, A. and Kartvelishvili, V. (1996). SVD approach to data unfolding. *Nuclear Instruments and Methods in Physics Research A*, 372:469–481.
- Kuusela, M. and Panaretos, V. M. (2015). Statistical unfolding of elementary particle spectra: Empirical bayes estimation and bias-corrected uncertainty quantification. *The Annals of Applied Statistics*, 9(3):1671–1705.
- Luenberger, D. G. (1969). *Optimization by Vector Space Methods*. John Wiley & Sons.
- Mathworks (2014). *Optimization Toolbox User’s Guide*. Release 2014a.
- Prosper, H. B. and Lyons, L., editors (2011). *Proceedings of the PHYSTAT 2011 Workshop on Statistical Issues Related to Discovery Claims in Search Experiments and Unfolding*, CERN-2011-006, CERN, Geneva, Switzerland.
- Reiss, R.-D. (1993). *A Course on Point Processes*. Springer-Verlag.
- Ruppert, D., Wand, M. P., and Carroll, R. J. (2003). *Semiparametric Regression*. Cambridge University Press.
- Schmitt, S. (2012). TUnfold, an algorithm for correcting migration effects in high energy physics. *Journal of Instrumentation*, 7:T10003.
- Shepp, L. A. and Vardi, Y. (1982). Maximum likelihood reconstruction for emission tomography. *IEEE Transactions on Medical Imaging*, 1(2):113–122.
- Stark, P. B. (1992). Inference in infinite-dimensional inverse problems: Discretization and duality. *Journal of Geophysical Research*, 97(B10):14055–14082.
- Vardi, Y., Shepp, L. A., and Kaufman, L. (1985). A statistical model for positron emission tomography. *Journal of the American Statistical Association*, 80(389):8–20.